

Decomposition of carbon/phenolic composites for aerospace heatshields: Detailed speciation of phenolic resin pyrolysis products

Torres-Herrador, Francisco; Eschenbacher, Andreas; Coheur, Joffrey; Blondeau, Julien; Magin, Thierry E.; Van Geem, Kevin M.

Published in:
Aerospace Science and Technology

DOI:
[10.1016/j.ast.2021.107079](https://doi.org/10.1016/j.ast.2021.107079)

Publication date:
2021

License:
CC BY-NC-ND

Document Version:
Accepted author manuscript

[Link to publication](#)

Citation for published version (APA):
Torres-Herrador, F., Eschenbacher, A., Coheur, J., Blondeau, J., Magin, T. E., & Van Geem, K. M. (2021). Decomposition of carbon/phenolic composites for aerospace heatshields: Detailed speciation of phenolic resin pyrolysis products. *Aerospace Science and Technology*, 119, Article 107079. <https://doi.org/10.1016/j.ast.2021.107079>

Copyright

No part of this publication may be reproduced or transmitted in any form, without the prior written permission of the author(s) or other rights holders to whom publication rights have been transferred, unless permitted by a license attached to the publication (a Creative Commons license or other), or unless exceptions to copyright law apply.

Take down policy

If you believe that this document infringes your copyright or other rights, please contact openaccess@vub.be, with details of the nature of the infringement. We will investigate the claim and if justified, we will take the appropriate steps.

Decomposition of carbon/phenolic composites for aerospace heatshields: detailed speciation of phenolic resin pyrolysis products

Francisco Torres-Herrador^{a,b,d,*}, Andreas Eschenbacher^d, Joffrey Coheur^{a,c,f},
Julien Blondeau^{b,e}, Thierry E. Magin^a, Kevin M. Van Geem^d

^a*von Karman Institute for Fluid Dynamics, 1640 Rhode-St-Genese, Belgium*

^b*Thermo and Fluid dynamics (FLOW), Faculty of Engineering, Vrije Universiteit Brussel (VUB), 1050 Brussels, Belgium*

^c*Université de Liège, Aerospace and Mechanical Engineering, Allée de la Découverte 9, 4000 Liège, Belgium*

^d*Laboratory for Chemical Technology (LCT), Faculty of Engineering and Architecture, Ghent University, 9000 Ghent, Belgium*

^e*Combustion and robust optimization (BURN), Vrije Universiteit Brussel (VUB) and Université Libre de Bruxelles (ULB), 1050 Brussels, Belgium*

^f*Institute of Mechanics, Materials and Civil Engineering (iMMC), Université catholique de Louvain, Place du Levant 2, 1348 Louvain-la-Neuve, Belgium*

Abstract

Thermal Protection Materials (TPM) such as carbon/phenolic composites are used to protect spacecraft structures from extreme conditions. This protection is, in part, achieved by the decomposition via pyrolysis of the phenolic resin. Finite rate chemistry models are however still unable to predict the chemical production rates and composition of the pyrolysis products accurately. This is mostly due to the scarcity of experimental data for model validation. In this work, the decomposition of a phenolic material representative of thermal protection material is studied in a unique micro-pyrolysis unit for the temperature range 300-800 °C. This unit is equipped with highly sensitive

*Corresponding author. fratorhe@vki.ac.be (F. Torres-Herrador)

detectors allowing us to identify and quantify products in a broad range of molecular weights up to 240 g mol^{-1} . More than 50 different products of the pyrolysis of phenolic resin have been quantified with a mass balance closure greater than 80 %. The major compound groups found are permanent gases, phenols as well as larger molecules such as diphenols and naphthalenes. In addition, the char yield obtained at the fast heating rates employed in our apparatus was found $\sim 5\%$ -points lower compared to traditional thermogravimetry.

Keywords: Carbon/phenolic composite, pyrolysis, gas chromatography

1. Introduction

In order to withstand the high thermal loads achieved during an atmospheric re-entry, most spacecraft use ablative Thermal Protection Materials (TPMs). This family of materials has been successfully used since the Apollo Program, even though there was a lower interest during the Space Shuttle program (1981-2011), when they were replaced by re-usable ceramic tiles. However, these materials have substantially evolved since the 1960s. State-of-the-art ablative materials, based on a short carbon fiber preform impregnated with phenolic resin, are known as carbon/phenolic composites [1]. The combination of these two materials leads to a highly porous, poorly conductive material which efficiently protects the spacecraft [2]. Moreover, when the phenolic resin gets heated to temperatures above $400 \text{ }^\circ\text{C}$ [3], it

This is a preprint of a peer-reviewed publication in Aerospace Science and Technology.

starts decomposing via pyrolysis, thereby releasing gases which percolate through the material and are ejected into the boundary layer providing a blockage effect of the incoming flow[4]. While the gas phase chemistry is relatively well understood, the knowledge of the pyrolysis process and the generation of pyrolysis gases is still limited, and most models rely on lumped, Arrhenius-*like* reactions. Multi-component parallel reactions [5–7] or more recently competitive reactions [8] are generally employed to model pyrolysis. These approaches usually rely on the elemental composition of the material and thermochemical equilibrium calculations to compute the actual composition of the gas mixture [9]. High-fidelity finite-rate chemistry models are still under development [6]. A better understanding of the pyrolysis process and of the products generated could lead to a better design of heat-shields, possibly reducing some of the safety margins currently used.

Several carbon/phenolic materials have been successfully applied to entry scenarios [10, 11], such as the Phenolic Impregnated Carbon Ablator (PICA[®]) from NASA, its Space-X variant (PICA-X[®]) or the European Asterm[®] from Airbus. In the present work, the ZURAM[®] material developed by the German Aerospace Agency (DLR) for research purposes was used [1]. This material is representative of the carbon/phenolic composite family and its data can be made publicly available without restrictions.

The analysis of the thermal degradation of phenolic resins used for spacecraft applications started back in 1967 with the work of Sykes [3]. He analyzed phenolic resin using different techniques such as Differential Thermal Analysis (DTA), Organic Elemental Analysis (OEA) or Gas Chromatography (GC). He [3] hypothesized some of the reactions occurring in the material,

based on previous works from Jackson and Conley [12] and from Ouchi and Honda [13]. However, technological limitations did not allow these researchers to identify the different compounds present in the mixture of pyrolysis gases, being limited to identification techniques based on retention time and injection of pure compounds for comparison. Later, Trick and Saliba [14, 15] combined Thermogravimetry Analysis (TGA) with Fourier-Transform Infrared Spectroscopy (FTIR) to characterize the evolution of pyrolysis products during a slow heating ramp of $1\text{ }^{\circ}\text{C min}^{-1}$. The understanding gained from these early works, based on the most prevalent products, was that the thermal decomposition process occurred in four distinct steps:

- Step 0 (0-350 °C): Outgassing of trapped gas and/or humidity.
- Step 1 (200-550 °C): Production of water and phenol due to the release of pendant groups from the backbone of the polymer.
- Step 2 (400-800 °C): CO and CH₄ are produced by mechanisms related to the decomposition of methylene bridges or carbonyl cross-links.
- Step 3 (> 750 °C): Unstable char rings fuse, forming graphite-like char and releasing H₂.

Two decades later, works of Wong et al. [16, 17] and Bessire et al. [18, 19] have re-ignited the interest to better understand the pyrolysis process of phenolic resins. On the one hand, Wong analyzed PICA using an in-house developed reactor, in which batches of 50 mg of sample material reacted for one hour at a given temperature in a step-wise pyrolysis, re-using the same sample at different temperatures. After each step, the reactor was quenched

with cold water and the gases were collected and analyzed off-line using different GC columns. Due to the large residence times and sample masses, secondary reactions are to be expected, thus hindering the understanding of finite-rate processes. On the other hand, Bessire et al. developed an interesting experimental facility based on the identification of products by means of on-line Time-Of-Flight Mass Spectrometry (TOF-MS)[18]. In this case, the sample was pyrolyzed using resistive heating (Joule effect) at high heating rates (up to $25\text{ }^{\circ}\text{C s}^{-1}$, much higher than traditional TGA), and the products were collected and continuously analyzed while they evolved. To avoid damaging the copper blocks that carried the electricity responsible of heating the sample, these were water cooled. This generated a large gradient of temperatures within the 25 mm long sample. While the temperature was measured at the centerline with a thermocouple, it is possible that part of the collected gases could arrive from other sections of the sample which were submitted to slower heating rates than the reported nominal value due to cooling. In addition, TOF-MS is sensitive to the molar yields. Therefore, compounds with high Molecular Weight (MW) but low yield are difficult to identify in such a unit.

The aim of this work is to better understand the decomposition of phenolic resin via pyrolysis and to understand the effect of the heating rate on the char formation. To do so, we try to achieve the best of both worlds [19, 20], having a great resolution in terms of compound identification and quantification, while still keeping relevant fast pyrolysis data at different temperatures. To do so, we employed a micro-pyrolysis furnace connected with a two-dimensional GC (GC×GC) coupled to TOF-MS for identification, and Fire Ionization

Detector (FID), Thermal Conductivity Detector (TCD), and Pulsed Discharge Detector (PDD) for quantification of compounds up to MWs on the order of 240 g mol^{-1} . Two types of tests are performed: 1) isothermal tests in which a sample is submitted to a given temperature, and 2) step-wise decomposition in which the same sample is re-used at different temperatures similar to Wong [16]. The use of sample sizes in the order of $200 \mu\text{g}$ allow us to assume isothermicity of the sample (Section 2).

2. Experimental Techniques

The unit used to perform these experiments is a flash pyrolysis reactor connected to a multitude of analytical measurement devices (Fig. 1) [21]. The pyrolysis reactor is a tandem of two resistively heated quartz reactors. In the first one, the pyrolysis of the solid material takes place. The second reactor is used to investigate gas phase chemistry (and cracking) if desired. In a typical experiment, the solid material ($m \approx 200 \mu\text{g}$) was loaded in a deactivated stainless steel cup and fixed at the top of the first reactor (outside the heated zone) to a sample holder. Once the reactor was heated to pyrolysis temperature, the sample was dropped in the heated zone. After the pyrolysis step, the gases were quickly swept away by helium carrier gas (105 mL min^{-1}) and trapped by a cryo-trap (liquid nitrogen, 77 K) which was used to retain the products while avoiding any further reactions. The cryo-trap stayed on for 5 min, and after being switched off, the products got released by heating up the GC oven. The GC oven was initially held at $0 \text{ }^\circ\text{C}$ for 6 min, then it was heated to $40 \text{ }^\circ\text{C}$ at 4 K min^{-1} , followed by heating to $300 \text{ }^\circ\text{C}$ at 5 K min^{-1} . The analysis section is composed by: 1) a 2-dimensional GC (GC \times GC, Rtx-PONA

50 m and BPX-50 2 m for 1st and 2nd dimension respectively) equipped with a FID and a TOF-MS, and 2) a customized GC with different detectors (TCD, PDD) to quantify permanent gases and other light compounds (H_2 , water, methanol, etc.) hereafter referred to as GC-TCD/PDD. The GC \times GC used a liquid CO_2 modulator, with 5 s modulation time. This configuration allows for the detection and quantification of the different products formed during the pyrolysis of a carbon/phenolic ablator.

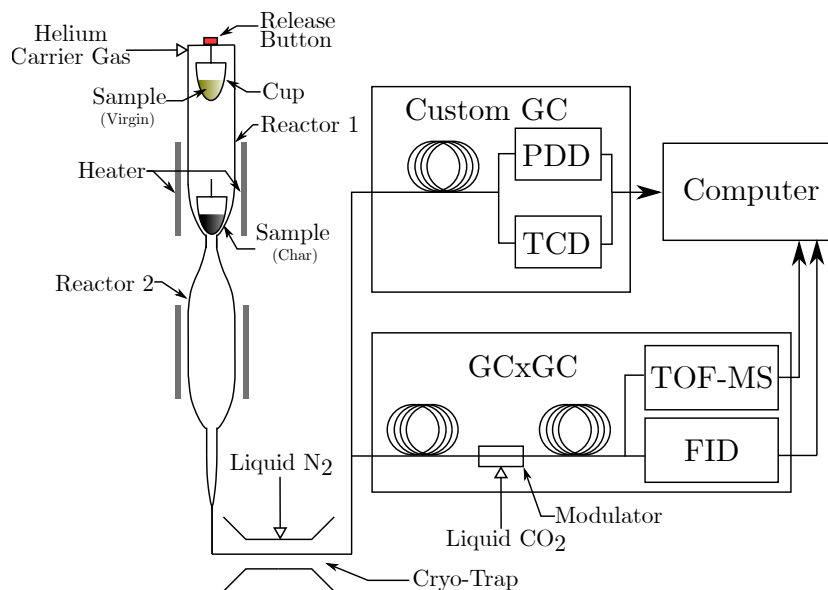


Figure 1: Schematic view of the micropyrolysis experimental unit.

The use of such small sample sizes has two main benefits: the sample will heat up more uniformly and rapidly to the pyrolysis temperature, and pyrolysis will be the driven phenomenon. This is verified by the use of three dimensionless numbers (Bi , Py^I , Py^{II}). For a typical experiment ($\sim 200 \mu g$)

of phenolic resin from ZURAM[®] at 700 °C:

$$\text{Bi} = \frac{t_{\text{cond}}}{t_{\text{conv}}} = \frac{L_c h}{\lambda_z} = 0.004 \quad (1)$$

$$\text{Py}^{\text{I}} = \frac{t_{\text{pyro}}}{t_{\text{cond}}} = \frac{\lambda_z}{\rho_z c_{p_z} L_c^2 \mathcal{A} \exp\left(\frac{-\mathcal{E}}{RT}\right)} = 4600 \quad (2)$$

$$\text{Py}^{\text{II}} = \text{Bi} \cdot \text{Py}^{\text{I}} = 21 \quad (3)$$

where L_c is the characteristic length of the sample cup, h is the heat transfer coefficient, the subindex z refers to ZURAM[®], λ_z is its thermal conductivity, ρ_z is the intrinsic density, c_{p_z} is the heat capacity, and $\mathcal{A} \exp\left(\frac{-\mathcal{E}}{RT}\right)$ is the kinetic rate [7, 22, 23]. The following assumptions can be taken if: 1) $\text{Bi} \ll 1$, sample can be considered isothermal, 2) $\text{Py}^{\text{I}} \gg 1$, heat transfer inside the sample is fast compared to pyrolysis, 3) $\text{Py}^{\text{II}} \gg 1$, heat transfer by convection is fast compared to pyrolysis ensuring same temperature as the furnace [24–26].

As it can be seen, Bi is much smaller than 1, ensuring a homogeneous temperature of the sample. Py^{I} greater than 1 indicates that the pyrolysis front is thick, thus the whole sample is undergoing pyrolysis at the same rate, in other words, the process is kinetically controlled. Finally, Py^{II} greater than 1 indicates that the sample reaches the pyrolysis temperature by convection quickly in comparison to the pyrolysis time, thus the assumption of the particle being at the same temperature of the furnace during pyrolysis is considered appropriate.

3. Methodology

3.1. Sample preparation

The material used to perform this study is the phenolic resin of the ZURAM[®] carbon/phenolic ablator [1]. Preliminary testing showed that the

carbon fibers in the material do not affect the pyrolysis product distribution, therefore it was decided to focus on the resin, thus achieving higher resolution.

The sample material was obtained from a slab of ZURAM[®], where an excess of resin did not impregnate the fibers, but it underwent the same preparation processes. The resin was then ground to powder in order to facilitate its manipulation. During the testing, it was stored in a glass vial in a desiccator to avoid humidity absorption.

With the sample material, we included fluoranthene as internal standard (Section 3.3) with varying mass throughout the different tests in the range from 1-7 μg . In addition, a small amount of quartz wool was added covering the sample in the cup to avoid any spillage, particularly during pyrolysis and to ensure that char remains in the cup to accurately determine its yield gravimetrically post-reaction. The quartz wool was torched before being introduced in the sample cup to remove any trapped humidity.

3.2. Experimental conditions

Two types of experimental tests were performed: isothermal tests and stepwise isothermal tests.

Isothermal tests were performed with a virgin sample at different temperatures, providing information of the products at those particular temperatures. This information is of great importance since the products that are produced at different temperatures may be different. Moreover, even though it is not possible to directly measure the heating rates at which the samples are pyrolyzed, we can certainly say from the non-dimensional numbers (Section 2) that they are much higher than other methods[7, 16, 18], in the order of 10^3 K s^{-1} [27], hence their relevance for atmospheric entry scenarios. In our

experiments, we focused on the range between 500-700 °C, where the maximum mass loss rate was observed in TGA [7]. The second reactor was kept at 300 °C, a temperature low enough to avoid further reactions, but high enough to avoid condensation on the reactor walls. In addition, we performed an additional test with the second reactor at 800 °C, to study the stability of high molecular weight compounds.

The second type of experiments consists of a stepwise isothermal test following a similar method as in the works by Wong et al. [16, 17]. In these cases, we used a single sample, with a larger mass (973 µg), subjecting it consecutively to several increasing temperatures. After each pyrolysis step, the sample was taken out from the reactor and weighed. This provided a TGA-like evolution. Ideally, a large number of steps would be required to actually reproduce the TGA curve, but in the current study we have limited it to 5 steps.

3.3. Quantification of pyrolysis products

Quantification requires identification and calibration. The identification of the pyrolysis products was performed by comparing the spectrum of each compound with the NIST Mass Spectral Library 2008 version [28]. In some cases, a unique match could not be found but rather several isomers. In those cases, the empirical formula is reported.

The different detectors used in the micropyrolysis unit result in different responses depending on the component that is detected. Therefore, in principle, for each of the components a calibration is required in order to correlate the detected signal to the corresponding mass yield.

In the case of the GC-TCD/PDD, which is used to quantify the permanent

gases, a C₂- mixture (Air Liquide, composition in Vol %: CO₂ 0.2, CO 1.2 , N₂ 2.4 , CH₄ 5.25, acetylene 0.3, ethane 16.25, ethylene 32.5, H₂ rest) was used. The calibration curves for each gas are reported in Supporting Information.

For the FID detector, two different calibration methods were applied: one based on an Internal Standard (IS) mixture which was used in every measurement and another based on an external phenol quantification. The IS was a mixture of fluoranthene and $\alpha - \text{Al}_2\text{O}_3$ in a mass proportion of 1:30. The use of this mixture is due to the need of diluting the fluoranthene to avoid the saturation of the detector while still having a good accuracy when measuring its mass.

The second calibration was based on one of the most relevant compounds in the material: phenol (99.9% purity). This compound was injected in the micropyrolyzer with different masses. Then, the mass was linearly related to the integrated blob volume. This curve allows to relate the peak volume of phenol found in any of the samples with its actual mass yield.

The use of two calibrations allows to have more reliability on the computed yields. However, since both approaches provided similar results and uncertainties only the results from using the phenol calibration are presented.

3.4. Yield calculation

The quantification of the mass yields is performed differently depending on the detector. For the GC-TCD/PDD, since every light gas has been calibrated, the quantification of the produced gases only required the integration of the areas and the application of the response factors from the corresponding

except N₂ and acetylene which were not found in the pyrolysis of phenolic.

linear calibration curve.

However, for the compounds detected by FID this is not feasible since more than 50 compounds were detected and in many cases they may not be available in pure form. Therefore, to quantify them, we used the so-called Molecular Response Factor (MRF) method [29]. For a compound c its MRF will be given by:

$$\text{MRF}_c = -0.071 + 0.000857\Delta H_{\text{comb}} + 0.127n_{\text{Benz}} \quad (4)$$

where n_{Benz} is the number of benzene rings presents in the molecule and the heat of combustion ΔH_{comb} is approximated as:

$$\Delta H_{\text{comb}} = 11.06 + 103.57N_{\text{C}} + 21.85N_{\text{H}} - 48.18N_{\text{O}} + 7.46N_{\text{N}}. \quad (5)$$

The N_i represents the number of atoms ($i = \text{C, H, O, N}$) in each molecule.

Then, for any compound, the mols produced (n_c) will be determined by the following formula:

$$n_c = \frac{V_c}{V_{\text{IS}}} \frac{\text{MRF}_{\text{IS}}}{\text{MRF}_c} n_{\text{IS}} \quad (6)$$

Where V_c and V_{IS} are the blob volumes of the compound being processed and of the internal standard respectively, and n_{IS} is the number of moles of the internal standard compound. The internal standard is simply defined as a compound for which the moles injected is known, either by introducing an external compound in the sample cup and pyrolyzing it together with the material of interest, or by an external calibration (Section 3.3).

From here, one can compute the mass (m_c) of any compound c and the corresponding mass yield (y_c) related to the initial mass of the sample (m_0)

as follows:

$$m_c = n_c \cdot \text{MW}_c \quad (7)$$

$$\%m_c = y_c = \frac{m_c}{m_0} \quad (8)$$

where MW_c is the molecular weight of the compound being studied.

3.5. Uncertainty assessment

Estimating the uncertainty in the measurements is important for two reasons. Firstly, it provides the level of confidence of the experimenter about the data, which can be assessed by performing several repetitions of the same conditions. Secondly, it is important for readers who are interested in developing computer models using the experimental data, for which the uncertainty in the measurements will play a significant role on the results [8]. The uncertainty associated with the pyrolysis products (permanent gases and vapors) and the char are presented in the following sections.

3.5.1. Pyrolysis products

Typically, each experimental condition is repeated three times in order to assess the uncertainty on the measurements [19, 21]. Performing three repetitions for each of the conditions rapidly increases the overall time and cost of the experimental campaign. However, the resulting uncertainties in the measurements can be large when a few number of repetitions are performed and these uncertainties need to be quantified rigorously.

For a given temperature T_j , $1 \leq j \leq n_T$, we assume that the measurements of any compound i (gas, vapour), $1 \leq i \leq n_c$, are independent Gaussian random variables $Y_{i,j,1}, Y_{i,j,2}, \dots, Y_{i,j,n_s}$ with $Y_{i,j,k} \sim \mathcal{N}(\mu_{i,j}, \sigma_{i,j}^2)$ of mean $\mu_{i,j}$

and variance $\sigma_{i,j}^2$. We denote by n_s the total number of repetitions (or samples) of the experiment given i, j . The measurements are called “realizations” and the k -th realization of $Y_{i,j,k}$ is denoted by $y_{i,j,k}$.

In practice, the mean $\mu_{i,j}$ and variance $\sigma_{i,j}^2$ are unknown but fixed (i.e. deterministic), and an empirical estimator for their value can be computed from

$$\bar{y}_{i,j} = \frac{1}{n_s} \sum_{k=1}^{n_s} y_{i,j,k}, \quad (9)$$

$$s_{i,j}^2 = \frac{1}{n_s - 1} \sum_{k=1}^{n_s} (y_{i,j,k} - \bar{y}_{i,j})^2. \quad (10)$$

These empirical estimators vary from one experiment to the other and in order to quantify this variability one can define, for instance, a 95% confidence interval for the mean $\mu_{i,j}$ (i.e. an interval that has 95% of chance of containing the true value of the unknown mean) as

$$\left[\bar{y}_{i,j} - \frac{t_{n_s-1,0.975} s_{i,j}}{\sqrt{n_s}}, \bar{y}_{i,j} + \frac{t_{n_s-1,0.975} s_{i,j}}{\sqrt{n_s}} \right], \quad (11)$$

where $t_{n_s-1,0.975}$ is the one-sided T -distribution with $n_s \geq 2$ degrees of freedom and probability 0.975 for which the values are provided in standard tables [30]. As a rule of thumb, the value of $t_{n_s-1,0.975}$ has already significantly decreased for n_s larger than 5 and provides good results for estimating the uncertainty in the mean, but it is intractable to do so for all temperatures.

In order to keep the experimental time and cost affordable while ensuring a good estimation of the uncertainties, the experiment was repeated 6 times for the case at 800 °C ($n_s = 6$) and only once at the other temperatures ($n_s = 1$). Therefore, at these other temperatures the formulas from Eq. 10 and Eq. 11 are not applicable for estimating the uncertainty in the means.

In order to estimate the uncertainties at the temperatures where the experiment is carried out only once, one possibility is to apply Bayes' theorem [31, 32]. Following the Bayesian perspective, the information on the uncertainties gained with the measurements at 800 °C can be incorporated as prior knowledge to obtain a posterior probability density function at the other temperatures and estimate the uncertainties for those measurements, that would not be possible otherwise. Moreover, a consequence of the Bayesian analysis is that the parameters $\mu_{i,j}$ and $\sigma_{i,j}$ are no longer defined by single, deterministic values but rather by a joint probability density function (the posterior).

The posterior density function on the uncertain parameters can be computed through Bayes' theorem [31]

$$\underbrace{\pi(\mu_{i,j}, \sigma_{i,j} | y_{i,j,1}, \dots, y_{i,j,n_s})}_{\text{Posterior}} \propto \underbrace{\pi(y_{i,j,1}, \dots, y_{i,j,n_s} | \mu_{i,j}, \sigma_{i,j})}_{\text{Likelihood}} \cdot \underbrace{\pi(\mu_{i,j}, \sigma_{i,j})}_{\text{Prior}}, \quad (12)$$

where the symbol \propto is interpreted to mean “proportional up to a normalization factor independent of the unknown parameters $\mu_{i,j}$ and $\sigma_{i,j}$ ”. The likelihood function depends on the parameters and provides the plausibility of the measurements. The prior probability density function quantifies any prior knowledge that we may know about the parameters and will be used to account for the information obtained from the measurements at 800 °C.

The information on the means and variances obtained at 800 °C will be incorporated into the prior distribution through the computation of the coefficient of variation (CV) such that it can be used at $T \neq 800$ °C. The CV is defined as the ratio between the empirical standard deviation and the

empirical mean, that is, for any compound i (gas, vapour),

$$CV_{i,j} = \frac{s_{i,j}}{\bar{y}_{i,j}}. \quad (13)$$

The CV provides information on the variability of the compound yield determination. In this case, we have chosen the $n_c = 26$ compounds with the highest product yield from the 6 repetitions at 800 °C to perform this study, representing 83.6% of the total FID mass yield.

If we assume that the FID detector does not have a particular preference for certain compounds, or that this preference is corrected by the use of the MRF method (Section 3.4), the CV is a quantity that, in principle, should be constant for every compound. However, due to other sources of uncertainty (e.g. sample mass measurement, FID detector precision or possible variabilities of the sample composition), this value will not be unique, but it is expected to be normally distributed. This can be observed in Fig. 2, where the sample data closely follows the normal distribution (solid line). Normality hypothesis was also assessed by means of the Shapiro–Wilk test. In this test, the null hypothesis states that the samples come from a normal distribution for a given confidence level α . If the p-value is greater than α , the null hypothesis cannot be rejected, and it can be assumed that the samples are normally distributed. In this case, for $\alpha = 0.05$, the computed p-value=0.359. Therefore, it can be assumed that CV is distributed normally with parameters $CV \sim \mathcal{N}(\overline{CV} = 0.2535, s_{CV} = 0.1105)$.

It is worth noting that one has to be careful with the problem of double use of data when computing the CVs and applying the Bayes’ theorem to get the posterior on $\mu_{i,j}$ at $T_j = 800$ °C. At this temperature, the CV for the compound i has to be computed from the $n_c - 1$ other components. Using

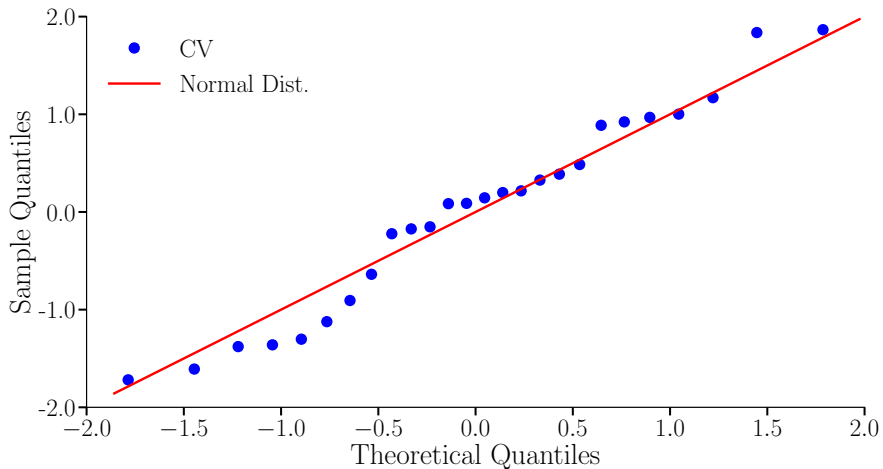


Figure 2: QQ-Plot representing the normalized distribution of CV for each compound of the 26 compounds considered (blue dots) and the standard normal distribution (red line).

the data both in the estimation of \overline{CV} and s_{CV} and in the likelihood could be problematic for small sample sizes, but should be less severe for larger sample size [32, 33]. At the other temperatures, all the CV values computed for the n_c compounds can be used safely.

We express the prior probability density function in Eq. (12) as

$$\pi(\mu_{i,j}, \sigma_{i,j}) \propto \exp \left(-\frac{1}{2} \left(\frac{\overline{CV} - \frac{\sigma_{i,j}}{\mu_{i,j}}}{\frac{s_{CV}}{\sqrt{n_c}}} \right)^2 \right), \quad (14)$$

which is a Gaussian distribution of known mean \overline{CV} and known standard deviation $s_{CV}/\sqrt{n_c}$. As it can be seen, a large number of compounds n_c used to estimate the distribution of CV (estimated from the case with repetitions) reduces the uncertainty associated with the measurements without repetitions. However, the uncertainties in the estimators \overline{CV} and s_{CV} are not included

in this analysis, but they are expected to be small thanks to the relatively higher value of n_c compared to n_s .

The likelihood function will be different whether we are at $T_j = 800^\circ\text{C}$ or not. At temperatures $T_j \neq 800^\circ\text{C}$, the likelihood function for the single production yield $y_{i,j,1}$ from the Gaussian distribution parameterized by its mean $\mu_{i,j}$ and variance $\sigma_{i,j}$ is:

$$\pi(y_{i,j,1}|\mu_{i,j}, \sigma_{i,j}) \propto \exp\left(-\frac{1}{2}\left(\frac{y_{i,j,1} - \mu_{i,j}}{\sigma_{i,j}}\right)^2\right). \quad (15)$$

At $T_j = 800^\circ\text{C}$, the likelihood is the product of the likelihoods for the single observations that are assumed to be independent:

$$\pi(y_{i,j,1}, \dots, y_{i,j,n_s}|\mu_{i,j}, \sigma_{i,j}) \propto \frac{1}{\sigma_{i,j}^{n_s}} \exp\left(-\frac{1}{2\sigma_{i,j}^2} [(n_s - 1)s_{i,j}^2 + n_s(\bar{y}_{i,j} - \mu_{i,j})^2]\right), \quad (16)$$

where $\bar{y}_{i,j}$ and $s_{i,j}$ are the empirical mean and variance computed from Eq. 9 and Eq. 10.

The posterior probability density function is obtained by injecting Eq. (15) or Eq. (16) with the prior Eq. (14) into Bayes' theorem Eq. (12), For instance, the resulting posterior for the mass yield of a given compound with a single measurement is written as:

$$\pi(\mu_{i,j}, \sigma_{i,j}|y_{i,j,1}) \propto \frac{1}{\sigma_{i,j}} \exp\left(-\frac{1}{2}\left(\frac{(y_{i,j,1} - \mu_{i,j})^2}{\sigma_{i,j}^2} + \frac{\left(\overline{CV} - \frac{\sigma_{i,j}}{\mu_{i,j}}\right)^2}{\frac{s_{CV}^2}{n_c}}\right)\right). \quad (17)$$

The posterior probability density function Eq. (17) provides a full description of the joint distribution for the mean and variance of the Gaussian model from which we assume that the measurements were distributed. From this

full distribution, we can then compute the marginal probability densities by integrating over the parameter set, as for instance for the mean:

$$\pi(\mu_{i,j}|y_{i,j,1}) = \int \pi(\mu_{i,j}, \sigma_{i,j}|y_{i,j,1}) d\sigma_{i,j}. \quad (18)$$

The expected value for the mean provided the measurement $y_{i,j,1}$ is the quantity defined as

$$\mathbb{E}(\mu_{i,j}|y_{i,j,1}) = \int \mu_{i,j} \pi(\mu_{i,j}|y_{i,j,1}) d\mu_{i,j}. \quad (19)$$

The expected value for the mean coincides with the single measurement value and the distribution is very close to a Gaussian distribution. To quantify the variability of the expected mean, the variance on the mean is computed as

$$\text{var}(\mu_{i,j}|y_{i,j,1}) = \int (\mu_{i,j} - \mathbb{E}(\mu_{i,j}|y_{i,j,1}))^2 \pi(\mu_{i,j}|y_{i,j,1}) d\mu_{i,j} \quad (20)$$

and will be used to quantify the uncertainty on the measurements. Finally, for a measurement condition j , the expected means and variances on the means for the mass yield will be given by adding the contributions from each compound:

$$\mathbb{E}(\mu_j|y_{i,j,1}) = \sum_{i=1}^{n_c} \mathbb{E}(\mu_{i,j}|y_{i,j,1}), \quad (21)$$

$$\text{var}(\mu_j|y_{i,j,1}) = \sum_{i=1}^{n_c} \text{var}(\mu_{i,j}|y_{i,j,1}). \quad (22)$$

Fig. 3 shows the results of the expected mean and standard deviation on the mean (the square root of Eq. (22)) as a function of the temperature. It can be seen that the case for which 6 repetitions were carried out (in orange) the uncertainty is smaller, while for the other cases, the uncertainty is larger. Despite the increased uncertainty, the trends are still clearly visible

and the number of measurements required is greatly reduced. In some cases, two measurements were performed for other cases at the same condition to ensure greater quality of the data. This information could also be used to reduce the uncertainties for those conditions, but doing so would not change the trends observed. Using the value of the variance as the measure of the uncertainty provides a $\sim 3.5\%$ variability for the cases of a single repetition. In summary, the Bayesian procedure described in this section allows to estimate uncertainties in the measurements even in the case of a single experimental repetition. This allows us to keep the time and the cost of the overall experiment campaign affordable while still providing a robust characterization of the uncertainties.

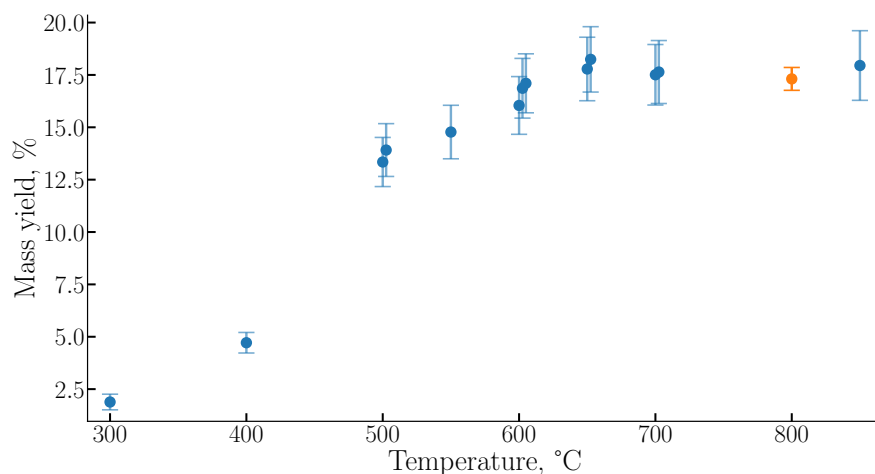


Figure 3: Expected means and standard deviations on the means of the volatiles mass yields quantified by FID using the information on the CVs at 800 °C. In orange, the case for which 6 measurements were performed, and in blue the cases with a single measurement. The values in temperature axis have been slightly moved for improved visualization.

3.5.2. Char measurements and uncertainties

The mass of the samples for both virgin and charred states is measured with a high precision balance ($\pm 1 \mu\text{g}$). However, for the determination of the uncertainty on the char yield mass measurement, another source of uncertainty is the intrinsic variabilities that the samples may have. Due to the small amount of material used during the determination and quantification tests, these two sources of uncertainties (material variability and balance precision) may become more relevant. Therefore, it was decided to run independent char determination tests in the same apparatus with significantly larger sample masses ($\sim 1 \text{ mg}$). This significantly improved the accuracy and repeatability of the char determination. Residual char measurements were performed at every tested temperature. Three additional measurements were performed at 500°C which provided a standard deviation of 2%. This value will be used for the other cases.

4. Results

4.1. Identification

A total of 53 different compounds have been identified from the pyrolysis of this phenolic resin. We have observed a number of permanent gases in the GC-TCD/PDD, namely: H_2 , CO , CO_2 , H_2O , CH_4 , C_2H_4 , C_2H_6 , NH_3 , $\text{C}_2\text{H}_3\text{N}$, and CH_2O . The list of vapor products (detected by FID) is indeed large (see Supplementary Information), but we observe that phenol, and some similar compounds are the major products (Fig. 4). In addition, we have observed compounds with large molecular weight, in most cases diphenols, but also naphthalenes and three fused rings (anthracene). Some of these high

molecular weight compounds also showed amines groups. This is relevant because previous studies on similar materials [17–19] did not report any compounds containing nitrogen. Even though the preparation of the material is often not publicly available, some authors mention that nitrogen containing compounds (hexamine, NH_4OH) are often used as catalyst in the synthesis of phenolic resins [13, 34].

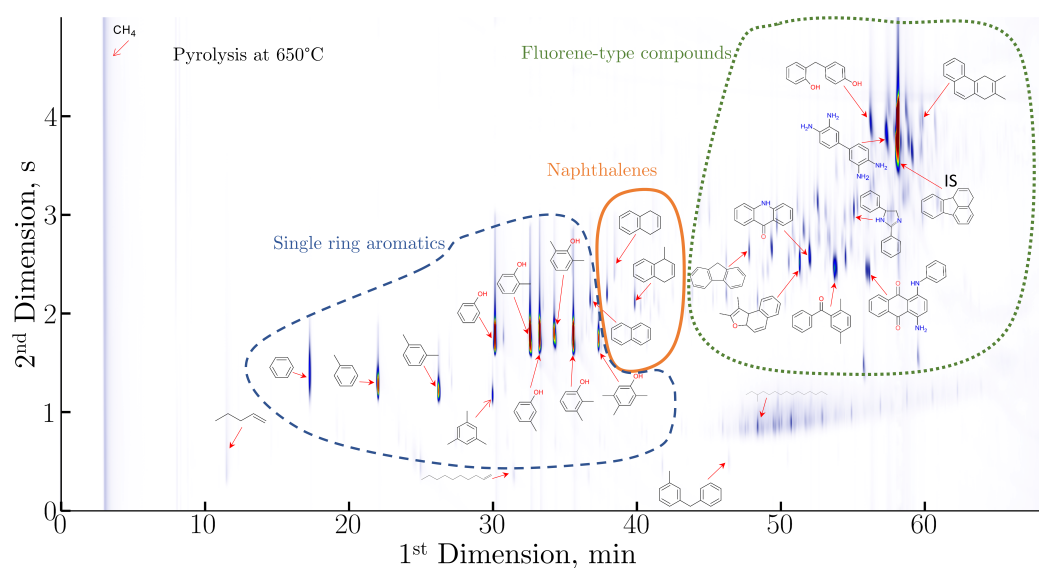


Figure 4: Identification of major compounds from pyrolysis of ZURAM[®] at 650 °C. The carbon number and boiling point increase with the first time dimension (min). The dashed blue line indicates the region in which single aromatic compounds and phenol derivatives elute. The solid orange line indicates the region of naphthalenes, and the dotted green line indicates heteroatom containing bisphenyls and polyaromatics (fluorene-type compounds).

4.2. Isothermal pyrolysis tests

The results of the isothermal tests are detailed in Fig. 5. It can be seen that the mass balance closes higher than 80 % for every case. The production

of light gases increases somewhat linearly as a function of temperature (Fig. 5). This is not the case for the vapors (FID) yields, which achieve a plateau at $\sim 650^\circ\text{C}$. This shows that at higher temperatures, the additional yield production results only in light gases. The char yield achieves a plateau at 800°C , which indicates that pyrolysis is mostly completed.

However, a decrease in the mass closure around temperatures close to the maximum rate of pyrolysis ($\sim 600^\circ\text{C}$) was observed. It appears that in these cases, the temperature was high enough to achieve a high degree of decomposition, but many of these products were of high MW (possibly $> 300\text{ g mol}^{-1}$). Such high molecular weight compounds may either have condensed on the reactor walls (see SI) or got trapped inside the GC column. However, at higher temperatures, these heavier products were broken into smaller compounds as was observed at $T_{\text{pyro}} > 700^\circ\text{C}$ which improved the mass balance by increasing the yield of low MW compounds with MW up to 90 g mol^{-1}).

This was also confirmed with a test in which the first reactor was kept at 600°C , while the secondary reactor temperature was increased up to 800°C (hereafter referred to as *Py@600°C, R@800°C* case), thus promoting further cracking of the high molecular weight compounds and therefore facilitating their quantification. In this case, we see that the gas yield increases considerably with respect to the other tests performed at 600°C (Fig. 5). This result indicates that the fact that the mass balance is not closed can be attributed to the formation of high MW compounds that could not be detected.

The production of NH_3 and other nitrogenated compounds are due to

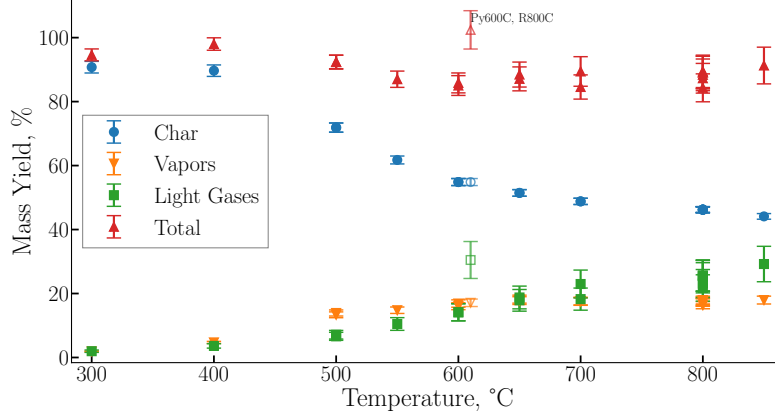


Figure 5: Mass balance of the isothermal tests. The *Py@600 °C, R@800 °C* test has empty symbols and has been moved slightly to the right for improved visualization.

the catalyst used in the production of the material (hexamine in the case of ZURAM®). This is confirmed by a relatively constant mass yield of 1.5 % of NH_3 for temperatures above 500 °C.

4.2.1. Comparison with elemental analysis

Design codes for heat shields [35, 36] track the elemental composition of the gases and then compute the equilibrium composition. Therefore, it is important that the elemental composition of the pyrolysis products resembles that of the one obtained through other means such as Organic Elemental Analysis [37]. Moreover, this comparison also validates our methodology for yield quantification. In the present case, the comparison has been carried out at 800 °C, for which we also performed elemental analysis of the char. Fig. 7 shows the results of this comparison. A good agreement for the elemental C, H, and N composition is observed; however, a larger discrepancy is found for oxygen. The result from micropyrolysis has been re-scaled to 100 % from

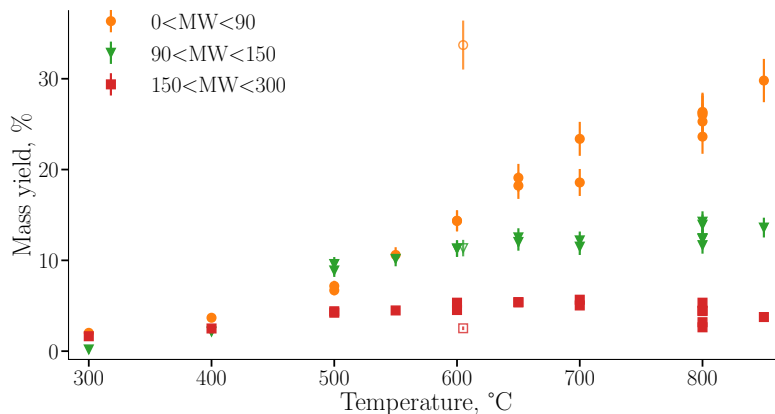


Figure 6: Comparison of mass yields for the different temperatures as for different molecular weight ranges. The empty dots are from the *Py*@600 °C, *R*@800 °C case.

a mass balance of $\sim 90\%$. As discussed above, many of the high molecular weight compounds that could not be detected due to their high MW may have contained nitrogen, thus reducing the proportion of oxygen, and consequently increasing C, H and N. It is also important to highlight that the char, even at this high pyrolysis temperature contained relevant percentages of the different elements (C: 96.36 %, N: 0.13 %, H: 0.08 %, O: 3.43 %), in contrast to the typical assumption of 100 % carbon in the char [6].

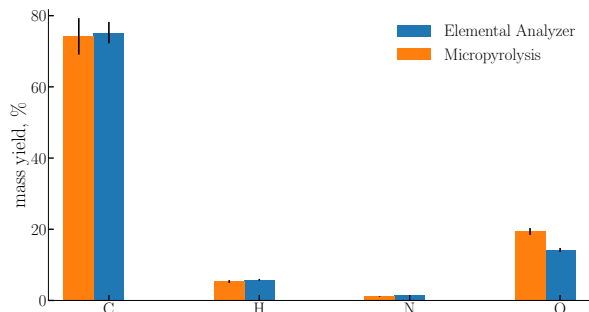


Figure 7: Comparison of elemental composition computed through the results of the current work, and from elemental analysis.

4.3. Stepwise pyrolysis tests

In these tests, the same sample is re-used at several temperatures similarly to Wong et al. [17]. At each step, the pyrolysis products were analyzed, and the sample mass was measured. In this case, five steps were performed.

Fig. 8a and 8b depict the evolution of the 10 most relevant compounds, in terms of their molar yields with respect to the initial sample mass. We can observe the “typical” 3-step evolution observed by other researchers [18]: 1) at low temperatures ($T < 550\text{ }^{\circ}\text{C}$), water and phenols are the most relevant products in mass yield, 2) in the central range ($550\text{ }^{\circ}\text{C} < T < 700\text{ }^{\circ}\text{C}$) CO , CO_2 , and H_2 gain importance, and 3) at high temperatures ($T > 750\text{ }^{\circ}\text{C}$) the production of H_2 becomes the most important product. We observe that in the range $400\text{-}650\text{ }^{\circ}\text{C}$ higher MW compounds are produced, while at higher temperatures, the MW of the compounds produced tends to decrease.

It can be seen (Fig. 9) that at low temperatures a large amount of compounds with high MW ($150\text{-}300\text{ g mol}^{-1}$) was produced; however, as temperature increases, compounds with smaller MW ($90\text{-}150\text{ g mol}^{-1}$) became

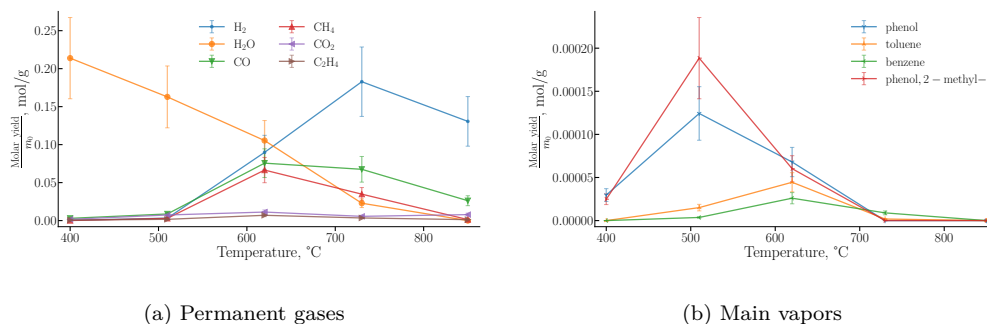


Figure 8: Evolution of the 10 main compounds for stepwise tests with temperature.

more relevant. Finally, at high temperatures ($T > 700$ °C), only permanent gases and small quantities of low MW compounds (lower than C₃) were produced.

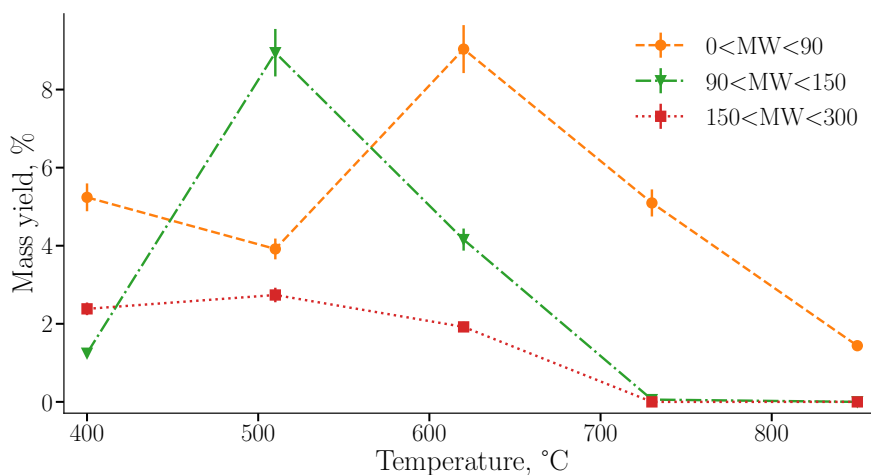


Figure 9: Evolution of the product yields for different ranges of MW for the stepwise decomposition tests.

At low temperatures, the main product is clearly H₂O, which may come from two sources: 1) trapped water in the pores from manufacturing or

absorbed from ambient humidity, or 2) product of the depolymerization reaction. Possibility 1) cannot be precisely assessed since no specific sample treatment was performed other than pulverizing the sample (Section 3.1) and storing it in a glass vial inside a desiccator. It is known that lightweight carbon/phenolic ablators are hydrophilic materials due to their nano-dispersed, high surface area phenolic resin [38]. Regarding possibility 2), it is known that during the first steps of the thermal degradation of phenolics, a cross-linking reaction occurs by which hydroxyl groups form a diphenyl ether group with the release of water [13]. Even though, we did not find the specific diphenyl ether in our MS identification of products, we found some similar compounds such as benzene, 2,4-dimethylbenzophenone, 1-methyl-2-(4-methylphenoxy)-, or 4,4'-dimethoxydiphenylmethane which could have been released in a further step after the formation of the diphenyl ether. A maximum production rate of these products was observed at 510 °C (see SI).

In this first range of temperatures (up to 600 °C), the production of phenol and some similar compounds (o-cresol, dimethylphenol, m-cresol) also achieved their maximum yield. This is mostly due to the release of pendant groups which are not part of the backbone of the polymer [39]. Bessire et al. [18] also found xylene in this range of temperature from their MS measurements, but argued that this assignment was ambiguous, and that the mechanism for its production is unknown. Our measurements also show production of m-xylene in the range 510-620 °C. The work of Mante et al [40] on lignin pyrolysis for production of simple phenols suggests that xylene may be produced by the deoxygenation of phenols.

CO₂ is the product of a decarboxylation reaction. In this reaction, a

free carboxyl group (COOH) may undergo secondary reaction with the right to produce CO₂ [40]. In the phenolic resin, this may occur in two different moments [19]: in the initial decomposition of the pristine resin, or in the decomposition of carboxyl groups formed by reactions with H₂O produced through condensation in a second step.

CO is produced from the first pyrolysis step at 400 °C, and it reaches its maximum at a subsequent pyrolysis temperature of 620 °C in our measurements. A pathway for the production of CO would be the decomposition of a carbonyl cross-link. This pathway was proposed by Ouchi [13] and then explored again by Bessire et al. [18] however, limitations on their MS did not allow to clearly identify the *parent* compound. In contrast, in our measurements, different benzophenone compounds were observed (2,4-dimethylbenzophenone, 2,5-dimethylbenzophenone) up to a pyrolysis temperature of 620 °C (see SI).

The production of CH₄ may be explained by two different mechanisms: a two-step mechanism from Ouchi [13], or a one-step mechanism from Trick and Saliba [14]. The first step from Ouchi [13] describes the formation of a methyl substituted benzene ring and a benzene from the reaction of hydrogen with the carbon cross-link, then hydrogen reacts again with the methyl substituted benzene to produce methane and benzene. This mechanism is well supported with our data since the production of CH₄ and benzene follow the same trends. The one-step mechanism from Trick and Saliba [14] proposes the decomposition of a methylene bridge due to the reaction with H₂. This mechanism also seems feasible from the observation of 1-benzyl-3-methylbenzene in our products (see SI). In particular, this

compound is observed at low temperatures 400-510 °C which may indicate that this one-step requires less energy to occur, while the two-step mechanism occurs at higher temperatures.

The production of H₂ seems mostly due to the carbonization mechanism proposed by Ouchi [13]. In this mechanism, the unstable char collapses forming a net of hexagonal carbons similar to that of graphite. This is justified by the observation of naphthalene, benzofuran, fluorene and anthracene in the products up to 730 °C. At higher temperatures (>850 °C), most of the phenolic resin has been converted to stable char, therefore only some remaining hydrogen is released without further release of polycyclic aromatic compounds.

4.3.1. Comparison with TGA

A comparison between the stepwise measurements and TGA data on phenolic resin [37] has also been performed. The TGA experiment was performed using a *STA 449 F3 Jupiter* (Netzsch) in argon atmosphere at 20 K/min with a purging gas of 50 ml/min and platinum crucibles with a pierced lid [7]. First, we can observe that the mass loss computed from the yields (FID and GC-TCD/PDD) accurately matches the results from char mass measurements (Fig. 10).

It can be seen that the trends from the stepwise measurements and TGA are in good agreement, but slightly lower char yields resulted for the stepwise measurements using the micropyrolyzer. In addition, in the central part of the decomposition 400-600 °C, one observes a larger difference. It seems that char production is related to the heating rate, as it is also in the pyrolysis of biomass [41–45]. At slow heating rates (traditional TGA), certain competitive reactions [8] in the pyrolysis of phenolic may produce char/residue already at

low temperatures, and only when temperature is higher, the more relevant mass loss occurs. Thus, the shift towards lower temperatures that can be observed in the graph.

On the opposite extreme, the mass loss evolution can also be computed from the char measurements performed for the isothermal tests (ie. using a new sample each time). In this case, the heating rate to achieve each temperature is high (in the order of 10^3 K s^{-1}). Therefore, such high heating rates reduce the char yield by ~ 5 percentage points compared to traditional TGA. The stepwise tests lie in between: at each step, the temperature is raised quickly, and kept for 5 min, such that the overall heating rate would be smaller than in the isothermal tests. Indeed, this is observed in the char yield evolution as it lies between the other two extremes Fig. 10.

This effect may be of great importance for the development of TPM for spacecraft since current models do not take a variable char yield into account, with the exception of competitive schemes [8]. In TPM, one may expect heating rates ranging from thousands of degrees per second for the part of the material facing the flow, to few degrees per minute for the deepest part of the heatshield [36].

5. Conclusion

This work provides novel data on the thermal degradation of the phenolic resin used in the ZURAM[®] TPM. The experiments have been performed in a custom set-up which allows for both identification and quantification of the pyrolysis products ranging from hydrogen to complex hydrocarbons of high molecular weight. The use of a single unit equipped with an extensive

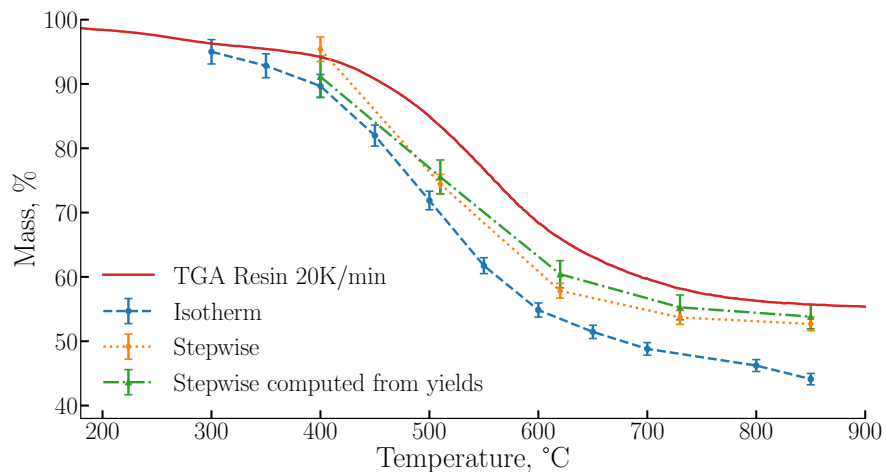


Figure 10: Comparison of mass loss curves obtained in this work with TGA data from Torres-Herrador et al. [37]

separation section and, in particular, the usage of a GC×GC system for on-line analyses results in a superior separation and a better quantification of the non-condensed products.

In our measurements, 53 different products of the pyrolysis of phenolics have been found. The major products are: water, CO, phenol and its derivatives, and methane. Many additional high molecular weight compounds such as diphenols and naphthalenes were quantified. The identification of these products has helped to confirm hypotheses on different reaction mechanisms regarding the production of the main products, for instance, the production of xylene.

The char yield determined by slow pyrolysis using a TGA was higher by $\sim 5\%$ -points compared to subjecting the sample to fast pyrolysis conditions in our unit. This confirms the need for more complex competitive models [8]

for the decomposition of phenolic resin that take the effect of the heating rate of the sample into account.

These data could be used for calibration of Arrhenius parameters of a given mechanism by simulating the pyrolysis process of phenolic resin for the different operating conditions of the experimental unit.

Acknowledgments

The research of F. Torres-Herrador is supported by SB PhD fellowship 1S58718N of the Research Foundation Flanders (FWO). We acknowledge Thomas Reimer and Christian Zuber (DLR Stuttgart) for valuable discussions on the material used in this work. The work of J. Coheur is supported by the Fund for Research Training in Industry and Agriculture (FRIA) 1E05418F provided by the Belgian Fund for Scientific Research (F.R.S.-FNRS). We would like to thank Alessandro Turchi (VKI) for his help with the definition of the testing campaign. The research leading to these results has received funding from the European Research Council under the European Union's Horizon 2020 research and innovation programme / ERC grant agreement n° 818607.

References

- [1] T. Reimer, C. Zuber, J. Rieser, T. Rothermel, Determination of the Mechanical Properties of the Lightweight Ablative Material Zoram, in: Processing, Properties, and Design of Advanced Ceramics and Composites II, Vol. 261 of Ceramic Transactions Series, 2018. doi: 10.1002/9781119423829.ch28.

- [2] F. Panerai, J. C. Ferguson, J. Lachaud, A. Martin, M. J. Gasch, N. N. Mansour, Micro-tomography based analysis of thermal conductivity, diffusivity and oxidation behavior of rigid and flexible fibrous insulators, *International Journal of Heat and Mass Transfer* 108 (2017) 801–811. doi:10/f95p4d.
URL <http://www.sciencedirect.com/science/article/pii/S0017931016327235>
- [3] G. F. Sykes, Decomposition Characteristics of a Char-Forming Phenolic Polymer Used for Ablative Composites., Tech. Rep. TN D-3810 (1967).
- [4] B. Helber, A. Turchi, J. B. Scoggins, A. Hubin, T. E. Magin, Experimental investigation of ablation and pyrolysis processes of carbon-phenolic ablators in atmospheric entry plasmas, *International Journal of Heat and Mass Transfer* 100 (2016) 810–824. doi:10.1016/j.ijheatmasstransfer.2016.04.072.
URL <http://www.sciencedirect.com/science/article/pii/S0017931015310243>
- [5] H. E. Goldstein, Pyrolysis Kinetics of Nylon 6–6, Phenolic Resin, and Their Composites, *Journal of Macromolecular Science: Part A - Chemistry* 3 (4) (1969) 649–673. doi:10.1080/10601326908053834.
URL <http://dx.doi.org/10.1080/10601326908053834>
- [6] J. Lachaud, J. B. Scoggins, T. E. Magin, M. G. Meyer, N. N. Mansour, A generic local thermal equilibrium model for porous reactive materials submitted to high temperatures, *International Journal of Heat*

- and Mass Transfer 108, Part B (2017) 1406–1417. doi:10.1016/j.ijheatmasstransfer.2016.11.067.
- [7] F. Torres-Herrador, V. Leroy, B. Helber, L. Contat-Rodrigo, J. Lachaud, T. Magin, Multicomponent Pyrolysis Model for Thermogravimetric Analysis of Phenolic Ablators and Lignocellulosic Biomass, *AIAA Journal* 58 (9) (2020) 4081–4089, publisher: American Institute of Aeronautics and Astronautics eprint: <https://doi.org/10.2514/1.J059423>. doi:10.2514/1.J059423.
URL <https://doi.org/10.2514/1.J059423>
- [8] F. Torres-Herrador, J. Coheur, F. Panerai, T. E. Magin, M. Arnst, N. N. Mansour, J. Blondeau, Competitive kinetic model for the pyrolysis of the Phenolic Impregnated Carbon Ablator, *Aerospace Science and Technology* 100 (2020) 105784. doi:10/ggm55f.
URL <http://www.sciencedirect.com/science/article/pii/S1270963819332031>
- [9] J. B. Scoggins, J. Rabinovitch, B. Barros-Fernandez, A. Martin, J. Lachaud, R. L. Jaffe, N. N. Mansour, G. Blanquart, T. E. Magin, Thermodynamic properties of carbon–phenolic gas mixtures, *Aerospace Science and Technology* 66 (2017) 177–192. doi:10/gd8dh9.
- [10] K. T. Edquist, B. R. Hollis, C. O. Johnston, D. Bose, T. R. White, M. Mahzari, Mars Science Laboratory Heat Shield Aerothermodynamics: Design and Reconstruction, *Journal of Spacecraft and Rockets* 51 (4) (2014) 1106–1124. doi:10.2514/1.A32749.
URL <https://doi.org/10.2514/1.A32749>

- [11] M. Stackpoole, S. Sepka, I. Cozmuta, D. Kontinos, Post-Flight Evaluation of Stardust Sample Return Capsule Forebody Heatshield Material, in: 46th AIAA Aerospace Sciences Meeting and Exhibit, American Institute of Aeronautics and Astronautics, 2008. doi:10.2514/6.2008-1202.
URL <https://arc.aiaa.org/doi/abs/10.2514/6.2008-1202>
- [12] W. M. Jackson, R. T. Conley, High temperature oxidative degradation of phenol-formaldehyde polycondensates, *Journal of Applied Polymer Science* 8 (5) (1964) 2163–2193. doi:10/cbfhmp.
URL <https://onlinelibrary.wiley.com/doi/abs/10.1002/app.1964.070080516>
- [13] K. Ouchi, H. Honda, Pyrolysis of coal. 1. Thermal cracking of phenolformaldehyde resins taken as coal models, *Fuel* 38 (4) (1959) 429–443.
- [14] K. A. Trick, T. E. Saliba, Mechanisms of the pyrolysis of phenolic resin in a carbon/phenolic composite, *Carbon* 33 (11) (1995) 1509–1515. doi:10.1016/0008-6223(95)00092-R.
URL <http://www.sciencedirect.com/science/article/pii/S000862239500092R>
- [15] K. A. Trick, T. E. Saliba, S. S. Sandhu, A kinetic model of the pyrolysis of phenolic resin in a carbon/phenolic composite, *Carbon* 35 (3) (1997) 393–401. doi:10.1016/S0008-6223(97)89610-8.
URL <http://www.sciencedirect.com/science/article/pii/S0008622397896108>

- [16] H.-W. Wong, J. Peck, R. E. Bonomi, J. Assif, F. Panerai, G. Reinisch, J. Lachaud, N. N. Mansour, Quantitative determination of species production from phenol-formaldehyde resin pyrolysis, *Polymer Degradation and Stability* 112 (2015) 122–131. doi:10.1016/j.polyimdegradstab.2014.12.020.
URL <http://www.sciencedirect.com/science/article/pii/S0141391014004534>
- [17] H.-W. Wong, J. Peck, J. Assif, F. Panerai, J. Lachaud, N. N. Mansour, Detailed analysis of species production from the pyrolysis of the Phenolic Impregnated Carbon Ablator, *Journal of Analytical and Applied Pyrolysis* 122 (2016) 258–267. doi:10/f9h46d.
URL <http://www.sciencedirect.com/science/article/pii/S016523701630211X>
- [18] B. K. Bessire, S. A. Lahankar, T. K. Minton, Pyrolysis of Phenolic Impregnated Carbon Ablator (PICA), *ACS Applied Materials & Interfaces* 7 (3) (2015) 1383–1395. doi:10/f62x9w.
URL <https://doi.org/10.1021/am507816f>
- [19] B. K. Bessire, T. K. Minton, Decomposition of Phenolic Impregnated Carbon Ablator (PICA) as a Function of Temperature and Heating Rate, *ACS Applied Materials & Interfaces* 9 (25) (2017) 21422–21437. doi:10.1021/acsami.7b03919.
URL <http://dx.doi.org/10.1021/acsami.7b03919>
- [20] H.-W. Wong, J. Peck, R. Edwards, G. Reinisch, J. Lachaud, N. N. Mansour, Measurement of pyrolysis products from phenolic polymer

thermal decomposition, in: 52nd Aerospace Sciences Meeting, American Institute of Aeronautics and Astronautics, 2015. doi:10.2514/6.2014-1388.

URL <http://arc.aiaa.org/doi/abs/10.2514/6.2014-1388>

- [21] L. Li, R. V. D. Vijver, G. Sribala, J. Weng, K. V. Geem, Pyrolysis Study of Cinnamaldehyde Model Compound with Analytical Py-gc×gc-fid/tof-ms, Chemical Engineering Transactions 80 (2020) 79–84. doi:10.3303/CET2080014.

URL <https://www.cetjournal.it/index.php/cet/article/view/CET2080014>

- [22] A. Turchi, B. Helber, F. Torres-Herrador, A. Fagnani, T. E. Magin, L. Chipperfield, F. Pascon, T. van Eekelen, H. Ritter, Ablative-material numerical-test international series (AblaNTIS): an experimental/numerical effort to support the validation of material thermal-response tools, in: International Conference on Flight vehicles, Aerothermodynamics and Re-entry Missions and Engineering, Monopoli, Italy, 2019.

- [23] F. Torres-Herrador, B. Helber, A. Turchi, S. Gorugantu, K. M. Van Geem, O. Chazot, T. Magin, J. Blondeau, Characterization of the thermal degradation of the carbon-phenolic materials: an experimental effort on the ZURAM ablator., in: International Conference on Flight vehicles, Aerothermodynamics and Re-entry Missions and Engineering, ESA Publications Division, Monopoli, Italy, 2019.

- [24] J. Blondeau, Investigation of pulverised biomass combustion: detailed

- modelling of particle pyrolysis and experimental analysis of ash deposition, Ph.D. thesis, Université catholique de Louvain (May 2013).
- [25] D. L. Pyle, C. A. Zaror, Heat transfer and kinetics in the low temperature pyrolysis of solids, *Chemical Engineering Science* 39 (1) (1984) 147–158. doi:10/c9244q.
URL <http://www.sciencedirect.com/science/article/pii/S0009250984801402>
- [26] S. Maduskar, G. G. Facas, C. Papageorgiou, C. L. Williams, P. J. Dauenhauer, Five Rules for Measuring Biomass Pyrolysis Rates: Pulse-Heated Analysis of Solid Reaction Kinetics of Lignocellulosic Biomass, *ACS Sustainable Chemistry & Engineering* 6 (1) (2018) 1387–1399. doi:10/gct7j4.
URL <https://doi.org/10.1021/acssuschemeng.7b03785>
- [27] J. Proano-Aviles, J. K. Lindstrom, P. A. Johnston, R. C. Brown, Heat and Mass Transfer Effects in a Furnace-Based Micropyrolyzer, *Energy Technology* 5 (1) (2017) 189–195, eprint: <https://onlinelibrary.wiley.com/doi/pdf/10.1002/ente.201600279>.
doi:<https://doi.org/10.1002/ente.201600279>.
URL <https://onlinelibrary.wiley.com/doi/abs/10.1002/ente.201600279>
- [28] S. E. Stein, NIST/EPA/NIH Mass Spectral Library (NIST 08) and NIST Mass Spectral Search Program (Version 2.0f) (2008).
- [29] J.-Y. de Saint Laumer, E. Cicchetti, P. Merle, J. Egger, A. Chaintreau,

Quantification in Gas Chromatography: Prediction of Flame Ionization Detector Response Factors from Combustion Enthalpies and Molecular Structures, *Analytical Chemistry* 82 (15) (2010) 6457–6462, publisher: American Chemical Society. doi:10.1021/ac1006574.

URL <https://doi.org/10.1021/ac1006574>

- [30] R. Hogg, J. McKean, A. Craig, *Introduction to Mathematical Statistics*, 7th Edition, Pearson, Boston, 2012.
- [31] A. Gelman, J. B. Carlin, H. S. Stern, D. B. Dunson, A. Vehtari, D. B. Rubin, *Bayesian Data Analysis*, 3rd Edition, Chapman and Hall/CRC, Boca Raton, 2013.
- [32] R. C. Smith, *Uncertainty Quantification: Theory, Implementation, and Applications*, SIAM, 2013, google-Books-ID: 4c1GAgAAQBAJ.
- [33] J. Berger, The case for objective Bayesian analysis, *Bayesian Analysis* 1 (2004) 1–17. doi:10.1214/06-BA115.
- [34] P. Johnston, E. Doyle, R. Orzel, Phenolics: A Literature Review of Thermal Decomposition Products and Toxicity, *Journal of the American College of Toxicology* 7 (2) (1988) 201–220, publisher: SAGE Publications. doi:10.3109/10915818809014520.
URL <https://doi.org/10.3109/10915818809014520>
- [35] T. van Eekelen, I. Cozmuta, A. Martin, J. Lachaud, Ablation Test Case 3, in: *6th Ablation Workshop*, Illinois, 2014.
- [36] J. B. E. Meurisse, J. Lachaud, F. Panerai, C. Tang, N. N. Mansour, Multidimensional material response simulations of a full-scale tiled

ablative heatshield, *Aerospace Science and Technology* 76 (2018) 497–511.
doi:10/gc4pgh.

URL <http://www.sciencedirect.com/science/article/pii/S1270963817323179>

- [37] F. Torres-Herrador, A. Turchi, K. M. Van Geem, J. Blondeau, T. E. Magin, Determination of heat capacity of carbon composites with application to carbon/phenolic ablators up to high temperatures, *Aerospace Science and Technology* (2020) 10doi:10.1016/j.ast.2020.106375.

URL <http://www.sciencedirect.com/science/article/pii/S1270963820310579>

- [38] A. D. Omidy, F. Panerai, J. R. Lachaud, N. N. Mansour, A. Martin, Effects of Water Phase Change on the Material Response of Low-Density Carbon-Phenolic Ablators, *Journal of Thermophysics and Heat Transfer* 30 (2) (2016) 473–478, publisher: American Institute of Aeronautics and Astronautics .eprint: <https://doi.org/10.2514/1.T4814>. doi:10.2514/1.T4814.

URL <https://doi.org/10.2514/1.T4814>

- [39] J. A. Parker, E. L. Winkler, The effects of molecular structure on the thermochemical properties of phenolics and related polymers, Tech. Rep. R-276, National Aeronautics and Space Administration, Washington, D.C. (1967).

- [40] O. D. Mante, J. A. Rodriguez, S. P. Babu, Selective defunctionalization by TiO₂ of monomeric phenolics from lignin pyrolysis into

simple phenols, *Bioresource Technology* 148 (2013) 508–516.
doi:10.1016/j.biortech.2013.09.003.

URL <http://www.sciencedirect.com/science/article/pii/S0960852413014260>

- [41] J. Blondeau, H. Jeanmart, Biomass pyrolysis at high temperatures: Prediction of gaseous species yields from an anisotropic particle, *Biomass and Bioenergy* 41 (2012) 107–121. doi:10/f3zmcx.

URL <http://www.sciencedirect.com/science/article/pii/S0961953412001043>

- [42] M. J. Antal, W. S. L. Mok, G. Varhegyi, T. Szekely, Review of methods for improving the yield of charcoal from biomass, *Energy & Fuels* 4 (3) (1990) 221–225, publisher: American Chemical Society. doi:10.1021/ef00021a001.

URL <https://pubs.acs.org/doi/abs/10.1021/ef00021a001>

- [43] A. Trubetskaya, P. A. Jensen, A. D. Jensen, M. Steibel, H. Spliethoff, P. Glarborg, Influence of fast pyrolysis conditions on yield and structural transformation of biomass chars, *Fuel Processing Technology* 140 (2015) 205–214. doi:10.1016/j.fuproc.2015.08.034.

URL <http://www.sciencedirect.com/science/article/pii/S0378382015301454>

- [44] A. Leth-Espensen, P. Glarborg, P. A. Jensen, Predicting Biomass Char Yield from High Heating Rate Devolatilization Using Chemometrics, *Energy & Fuels* 32 (9) (2018) 9572–9580, publisher: American Chemical

Society. doi:10.1021/acs.energyfuels.8b02073.

URL <https://doi.org/10.1021/acs.energyfuels.8b02073>

- [45] J. Yu, N. Paterson, J. Blamey, M. Millan, Cellulose, xylan and lignin interactions during pyrolysis of lignocellulosic biomass, *Fuel* 191 (2017) 140–149. doi:10.1016/j.fuel.2016.11.057.

URL <http://www.sciencedirect.com/science/article/pii/S0016236116311589>